JACS
JOURNAL OF THE AMERICAN CHEMICAL SOCIETY
Article
Cite This: J. Am. Chem. Soc. XXXX, XXX, XXX−XXX
pubs.acs.org/JACS

Examining the Effects of Monomer and Catalyst Structure on the Mechanism of Ruthenium-Catalyzed Ring-Opening Metathesis Polymerization

William J. Wolf, Tzu-Pin Lin, and Robert H. Grubbs*

The Arnold and Mabel Beckman Laboratory of Chemical Synthesis, Division of Chemistry and Chemical Engineering, California Institute of Technology, Pasadena, California 91125, United States

Supporting Information

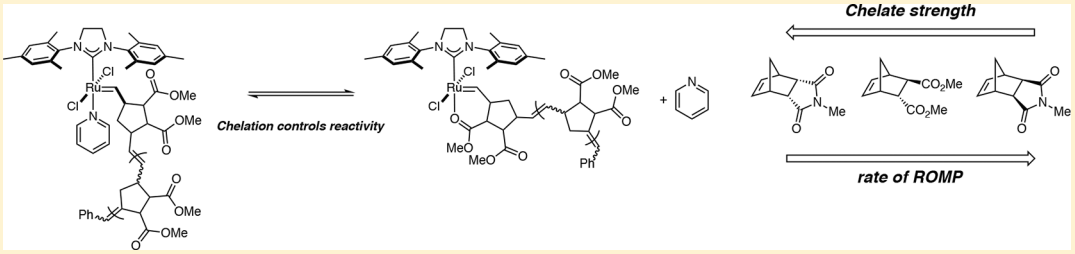

ABSTRACT: The mechanism of Ru-catalyzed ring-opening metathesis polymerization (ROMP) is studied in detail using a pair of third generation ruthenium catalysts with varying sterics of the N-heterocyclic carbene (NHC) ligand. Experimental evidence for polymer chelation to the Ru center is presented in support of a monomer-dependent mechanism for polymerization of norbornene monomers using these fast-initiating catalysts. A series of kinetic experiments, including rate measurements for ROMP, rate measurements for initiation, monomer-dependent kinetic isotope effects, and activation parameters were useful for distinguishing chelating and nonchelating monomers and determining the effect of chelation on the polymerization mechanism. The formation of a chelated metallacycle is enforced by both the steric bulk of the NHC and by the geometry of the monomer, leading to a ground-state stabilization that slows the rate of polymerization and also alters the reactivity of the propagating Ru center toward different monomers in copolymerizations. The results presented here add to the body of mechanistic work for olefin metathesis and may inform the continued design of catalysts for ROMP to access new polymer architectures and materials.

INTRODUCTION

Olefin metathesis is an indispensable synthetic tool and is used in a wide range of disciplines, from organic synthesis to materials science.[1] In particular, Ru-catalyzed metathesis is remarkably tolerant of a wide variety of functional groups and conditions, and Ru metathesis catalysts have seen extensive use in a myriad of applications. The ligands supporting the Ru center can be tuned to imbue certain desirable properties to the catalyst. From the parent first generation Ru catalyst **1**, substituting an N-heterocyclic carbene (NHC) ligand makes the catalyst more active[2] (**2**), a chelating benzylidene ligand makes the catalyst precursor more robust[3,4] (**3**), cyclometalated catalysts can be used for Z-selective metathesis[5,6] (**4**), and labile L-type ligands allow for rapid initiation or substitution[7,8] (**5**) (Figure 1). The fast-initiating third generation Ru catalysts like **5** are commonly used in polymer synthesis and they catalyze the polymerization of cyclic olefins in living fashion, allowing for a wide variety of uses in polymer and material science.[9]

The mechanism of Ru-catalyzed olefin metathesis has been studied in detail,[10] and its general features are well-established.[1] For phosphine ligated first and second generation Ru catalysts, the dissociation of one L-type ligand generates a reactive 14-electron fragment that undergoes olefin binding, cycloaddition, and cycloreversion to complete a single olefin metathesis event. The third generation Ru catalyst has also been studied in detail, both experimentally[7,8,11,12] and computationally,[13] and several distinct features of the mechanism have been observed. For small, monosubstituted olefins like 1-butene or ethyl vinyl ether, an associative mechanism was proposed on the basis of computational work by Grela and supported experimentally in a study of initiation of DMAP ligated catalysts with ethyl vinyl ether.[14] For bulkier olefins, such as 2-butene, a dissociative mechanism was proposed that is identical to the well-established mechanism by which second generation Ru catalysts operate. Slugovc and co-workers demonstrated that the structure of the monomer has a profound effect on the rate of polymerization and the structure of the propagating Ru species, as the growing polymer chain can chelate to the metal center.[11] More recently, Matson and co-workers expanded upon this by using macromonomers with varied ability to chelate to the Ru center.[15] Faster polymerizations were realized by using

Received: August 15, 2019

DOI: 10.1021/jacs.9b08835
J. Am. Chem. Soc. XXXX, XXX, XXX−XXX

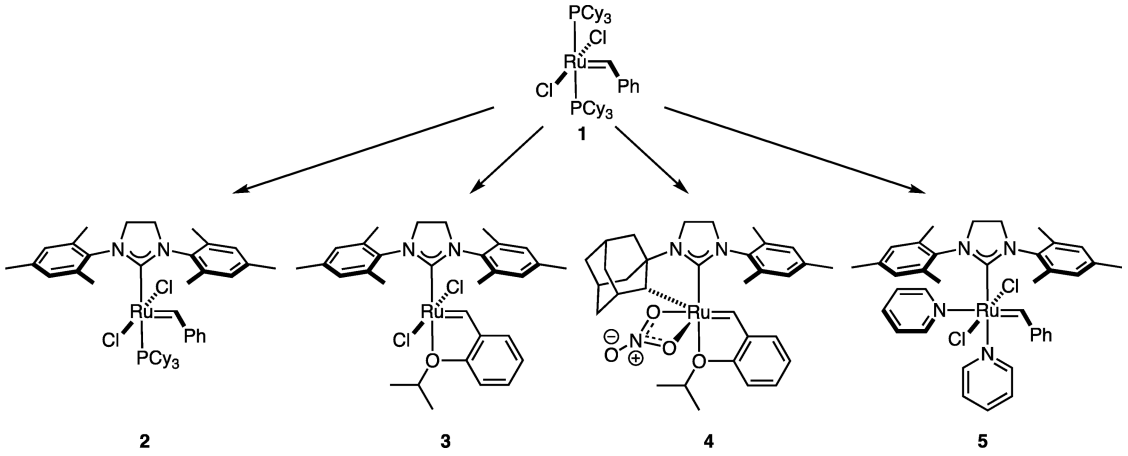

Figure 1. Several Ru catalysts with tailored ligands that affect their reactivity or selectivity.

monomers that are less prone to chelation. Guirronet and co-workers also showed that third generation Ru catalysts exist as five-coordinate complexes in solution after the dissociation of one of the pyridine ligands. This led to a unexpected zero-order dependence on catalyst concentration for ROMP.[12] We found computational evidence in support of these phenomena in our recent work on variably grafted bottlebrush polymers.[16]

In continuing our study of Ru-catalyzed ROMP, we have found experimental evidence for a number of important mechanistic features. Using a pair of sterically differentiated third generation Ru catalysts, we have found that norbornene monomers can be classified based on their ability to chelate to the Ru center and slow the rate of polymerization. Fast ligand exchange results in a steady-state concentration of the archetypal 14-electron Ru alkylidene. The mechanistic features described here may help in designing new synthetic sequences for making tailored polymers with catalyst control instead of substrate control.

RESULTS AND DISCUSSION

Two different third generation Ru catalysts were prepared with varying steric profiles, using the NHCs 1,3-Bis(2,4,6-trimethylphenyl)-4,5-dihydroimidazol-2-ylidene (SIMes, **5**) and 1,3-Bis(2,6-diisopropylphenyl)-4,5-dihydroimidazol-2-ylidene (SIPr, **6**[17]), as shown in Figure 2.

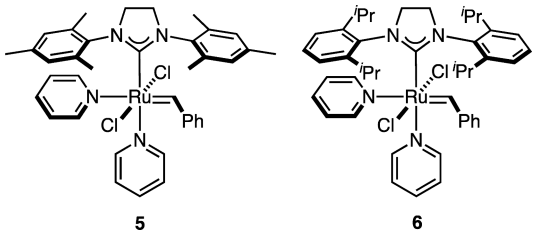

Figure 2. Two third generation Ru catalysts containing NHCs with differing steric bulk.

The solution-state behavior of each catalyst was examined by ^{1}H NMR. Guironnet and co-workers reported that **5** loses a pyridine ligand upon dissolution and the predominant species in solution is the monopyridine complex **5a**. They determined the dissociation constant (K_1) for **5** to be 0.5 using variable temperature NMR.[12] Based on this precedent, we found that **6** also gave the monopyridine complex **6a** in solution at 25 °C (Scheme 1); the five-coordinate complex has been independently prepared and characterized to confirm its assignment. For

Scheme 1

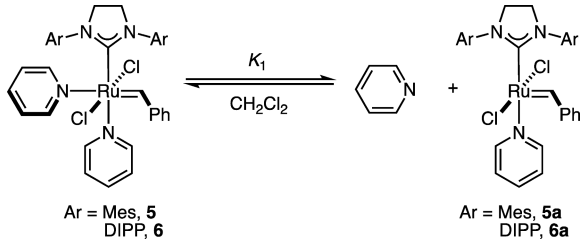

6, we attempted to measure K_1 using VT NMR: in CD_2Cl_2 at −90 °C, two broad benzylidene resonances were observed at δ 19.4 and 18.6 ppm for the bis and monopyridine species, respectively.

The addition of pyridine (3 equiv) to a CD_2Cl_2 solution of **6** at −90 °C shifted the equilibrium to the bispyridine complex and confirmed our assignment of each species. We were able to construct a van't Hoff plot over the range −130 °C to −100 °C (Figure 3) using the low-freezing $CDCl_2F$ as solvent and extrapolated these data to estimate K_1 = 11 at 25 °C.

The larger K_1 of **6** compared to **5** was attributed to the increased steric bulk of SIPr (relative to SIMes) that discourages ligand binding *trans* to the benyzlidene ligand. At catalytically relevant concentrations (typically <0.1 mM) this first equilibrium is large enough so that >99% of the Ru species in solution is five-coordinate. The frequency of pyridine exchange was measured using exchange spectroscopy (EXSY)[18] and showed an effect from the NHC, with a higher frequency of exchange observed for **5** than for **6**. Activation entropy for a second-order ligand exchange process is closer to zero for **5** ($\Delta S^{\ddagger}$ = 4 ± 6 J/mol·K) than for **2** ($\Delta S^{\ddagger}$ = +13 ± 6 J/mol·K, first-order ligand exchange) and was not consistent with an exclusively dissociative mechanism. The activation entropy for pyridine exchange of **6** was more negative ($\Delta S^{\ddagger}$ = −15 ± 6 J/mol·K) while both complexes exhibited similar $\Delta H^{\ddagger}$ (**5** = 10.5 ± 0.4 and **6** = 10.0 ± 0.4 kcal/mol). The synthesis of **5** from **2** by ligand exchange between PCy_3 and pyridine was speculated to operate via an associative pathway, and was attributed to the smaller size of pyridine relative to PCy_3.[7] The rate of exchange increases in the presence of higher

DOI: 10.1021/jacs.9b08835
J. Am. Chem. Soc. XXXX, XXX, XXX−XXX

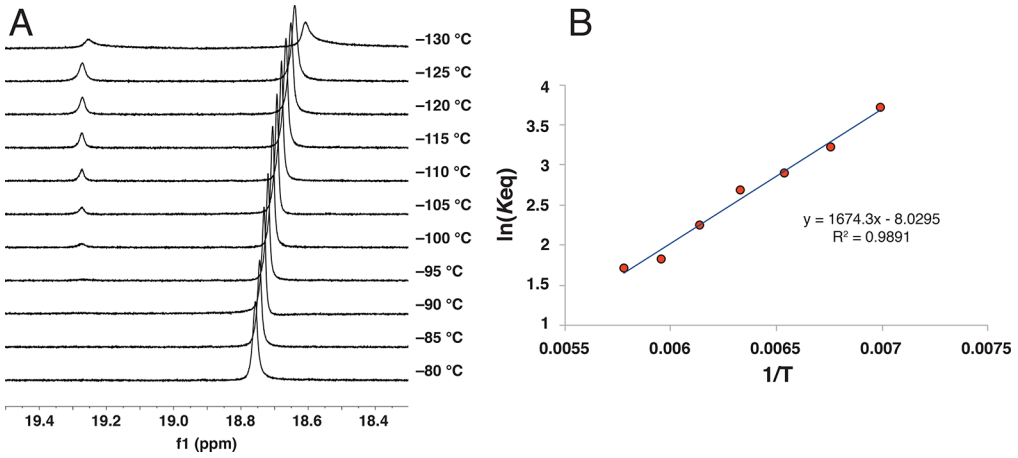

Figure 3. (A) Low temperature ^{1}H NMR array of **6** in $CDCl_2F$ solution showing both the mono- (δ 18.8 ppm) and bispyridine (δ 19.3 ppm) species. (B) The corresponding van't Hoff plot for the equilibrium between **6** and **6a**.

concentration of pyridine, further indicating that an associative exchange pathway is viable.

We next investigated the dissociation of pyridine from the five-coordinate complexes **5a** and **6a** (Figure 4) by

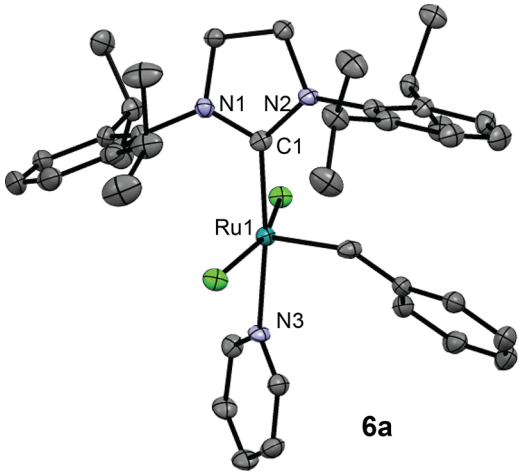

Figure 4. Solid state structure of **6a**. Ellipsoids are drawn at the 50% probability level and hydrogen atoms have been omitted for clarity. C, black; N, blue; Cl, green; Ru, teal.

competitively trapping the pyridine with a Lewis acid. The equilibrium for the dissociation of pyridine (K_2, Scheme 2) to generate the 14-electron fragment **7** can be calculated from the overall equilibrium and the equilibrium for the reaction of pyridine with the trapping reagent. We chose BPh_3 as the trapping reagent because it was appreciably Lewis acidic. The binding constant for pyridine to an analogous planar triaryl borane has been measured to be $2.7(2) \times 10^7$ M^{-1} in CH_2Cl_2.[19] When **5a** and 1 equiv of BPh_3 were mixed in CD_2Cl_2 solution, two new benzylidene resonances were observed at δ 18.4 and 16.8 ppm at −10 °C (Figure 5A). Upon warming to 25 °C, a ^{1}H−^{1}H EXSY experiment showed exchange between the two peaks (Figure 5B). We hypothesized that these new benzylidene resonances could be assigned to the μ-Cl bridged complexes **8a** and **8b** (Figure 5). Similar dimeric Ru complexes have been observed as both decomposition products of Ru metathesis catalysts[20,21] and metathesis active complexes.[22] A DOSY NMR experiment showed that both benzylidene peaks corresponded to complexes with smaller diffusion coefficients than that of the parent monopyridine complex **5a** by a factor of 1.2, and a mass corresponding to a dimer could also be detected by ESI-MS (m/z = 1136 Da). When **6a** was treated with BPh_3, only a single new benzylidene resonance was observed at δ 18.3 which also corresponded to a species with a smaller diffusion coefficient than **6a** as measured by DOSY NMR. The addition of pyridine to the reaction mixtures regenerated either **5a** or **6a**, indicating that the complexes were configurationally stable and that BPh_3 did not react deleteriously with either complex.

These dimeric species could also be generated using (2,6-di*tert*-butylpyridinium)tetrafluoroborate[23,24] as the pyridine trap or by the reaction of styrene with Piers' second generation Ru phosphonium alkylidene. These complexes have not been unambiguously characterized, but they indicate the highly reactive and Lewis acidic nature of the 14-electron intermediate and complicate the calculation of the dissociation of pyridine from the five-coordinate complexes. Based on these results, we have shown that **5a** and **6a** exhibit Lewis acidities similar to that of BPh_3 or (2,6-di-*tert*-butylpyridinium)tetrafluoroborate (Table 1) and so K_2 is estimated to be on the order of 10^{-6} M^{-1}.

The rate of pyridine trapping by either BPh_3 or (2,6-di-*tert*-butylpyridinium)tetrafluoroborate (rate of consumption of **5a** or **6a**) was nearly instantaneous, even at −78 °C. The reaction with BPh_3 could only occur by dissociation of the pyridine ligand from the Ru complex, evidence that the formation of the 14-electron species can proceed by a dissociative mechanism, in analogy to second generation Ru metathesis catalysts.

The reactivity of each complex for ROMP was evaluated by measuring the rates of polymerization for a series of norbornene monomers. Each complex was a competent

Scheme 2

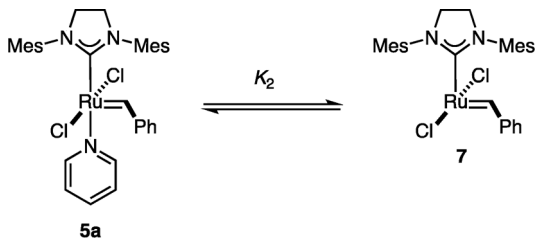

DOI: 10.1021/jacs.9b08835
J. Am. Chem. Soc. XXXX, XXX, XXX−XXX

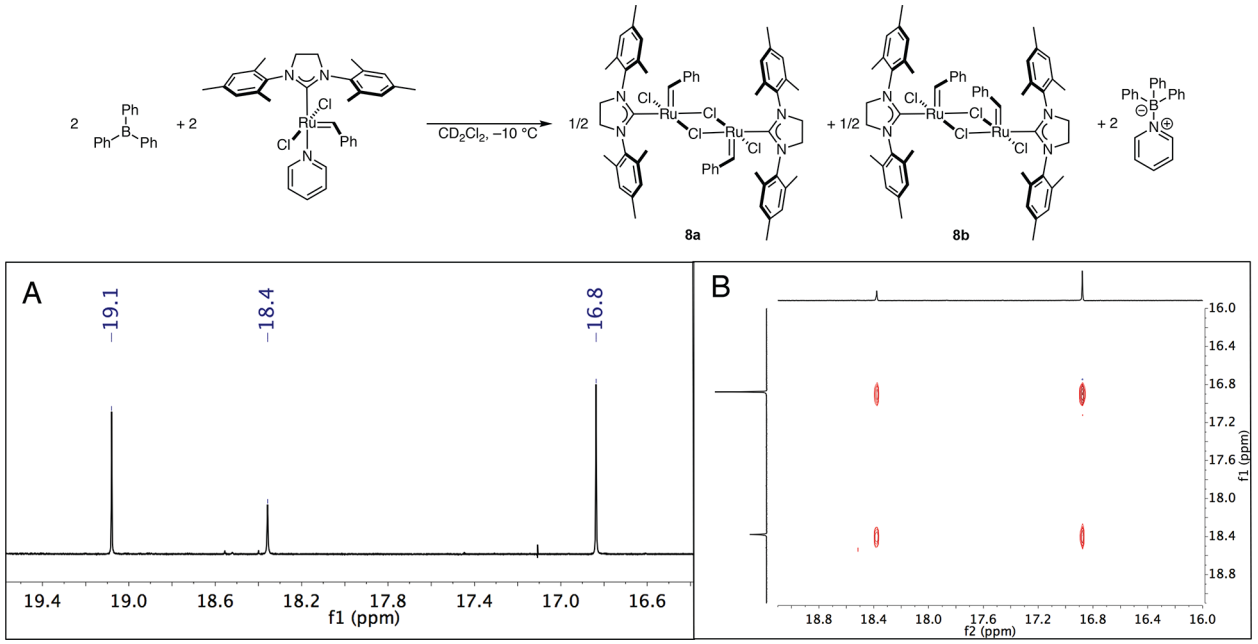

Figure 5. Dimerization of the 14-electron Ru bezylidene species in the presence of BPh_3 as indicated by the formation of two new species in the ^1H NMR (A) which exchange with one another as detected by EXSY (B).

Table 1. Equilibrium Constants for Pyridine Dissociation, K_1 and K_2, for Each Catalyst at 25 °C

	5	6
K_1	0.5 M^{-1}	11 M^{-1}
K_2[a]	~10^{-6} M^{-1}	~10^{-6} M^{-1}

[a]Estimates of K_2 based on the Brønsted acidity of (2,6-di-*tert*-butylpyridinium)tetrafluoroborate and a dimerization constant of 100.

catalyst for the polymerization of these monomers, providing both linear and bottlebrush polymers with excellent control of molecular weight. The rate constants for the homopolymerization of different types of monomers are shown in Table 2: all monomers exhibited first-order behavior for more than 5 half-lives. These data showed several interesting trends. For certain monomer types, the rates of polymerization showed a strong dependence on the structure of the catalyst, where the polymerization catalyzed by **6** was slower than that of **5**. These monomers were all diester monomers of *exo-exo* (*xx* prefix), *endo-exo* (*dx* prefix), or *endo-endo* (*dd* prefix) geometry. Other monomers showed a much weaker dependence of the rate of polymerization on the catalyst structure: these monomers were all of the *exo*-imide type, ***xx*-NMI** ***xx*-NPI**, or the macromonomers **PS**, **PLA**, or **PDMS**. *endo*-2,3-Dimethyl-5-norbornene (***dd*-DMN**) polymerizes very rapidly at 25 °C (full conversion in less than 15 s), but at 0 °C the rates of polymerization were similar for both complexes.

To probe the structure of the propagating Ru center, we reacted each catalyst with 10 equiv of different monomers at [Ru] = 0.02 M in CD_2Cl_2. Both **5** and **6** exhibit two distinct resonances for the ortho protons of pyridine: a free pyridine and a bound pyridine as established by Guironnet and co-workers. Similarly, when **5** is treated with 10 equiv of ***dd*-DMN**, two distinct pyridine resonances are observed at 25 °C. These resonances were assigned to the polymer-bound Ru center **5b-*dd*-DMN**, analogous in structure to **5** (Figure 6A). In contrast, the reaction of **5** and the diester monomer ***xx*-DME** gave only a single pyridine resonance at 25 °C. Its broad shape was indicative of a rapid exchange of pyridine between the free and bound states. This phenomenon is observed after all of the monomer has been consumed, precluding its attribution to monomer coordination to the Ru center. Instead, we assign this behavior to a rapid and reversible chelation by the polymer chain, as shown in the structure **5c-*xx*-DME** as shown in Figure 6B. Upon cooling, the resonance resolved itself into two signals, again corresponding to a free and a bound pyridine for **5b-*xx*-DME** (Figure 6B). In the absence of a Lewis basic moiety in the monomer, the resting state of the active Ru species is a five-coordinate pyridine adduct. If the monomer is substituted with a Lewis basic site such as an ester, it competes with pyridine to bind to the metal center. Slugovc and co-workers observed this same phenomenon when using the first and third generation Ru catalysts as initiators for ROMP. Our recent work on variably grafted brush polymers also identified chelation as an important factor controlling the rates of polymerization of norbornene monomers.[16]

Several different types of common norbornyl monomers were analyzed in analogous fashion and classified as either "chelating" or "nonchelating," as shown in Figure 6C (see Supporting Information (SI) for ^1H NMR spectra). The chelating monomers are comprised of the diester monomers of all three stereochemical types, with the *endo*, *endo* isomers demonstrating the strongest chelation. The geometric orientation of the *endo* substituents is likely responsible for their propensity to chelate to the Ru center. For **5**, the exoimide group (e.g., ***xx*-NMI**) does not chelate to the Ru center (even at [Ru] = 0.05 mM), as observed for both small molecule monomers and the PDMS macromonomer. Similar solution-state behavior was also observed for **6** with both monomer types.

We used the dimethyl ester monomer series (***xx*-DME**, ***dx*-DME**, and ***dd*-DME**) to probe the effect of stereochemical configuration on the chelating behavior. The Ru catalysts were reacted with 10 equiv of a particular monomer to form an

DOI: 10.1021/jacs.9b08835
J. Am. Chem. Soc. XXXX, XXX, XXX−XXX

Table 2. Measured Homopolymerization Rate Constants for a Series of Geometrically Differentiated Monomers Using 5 and 6 at 25 °C

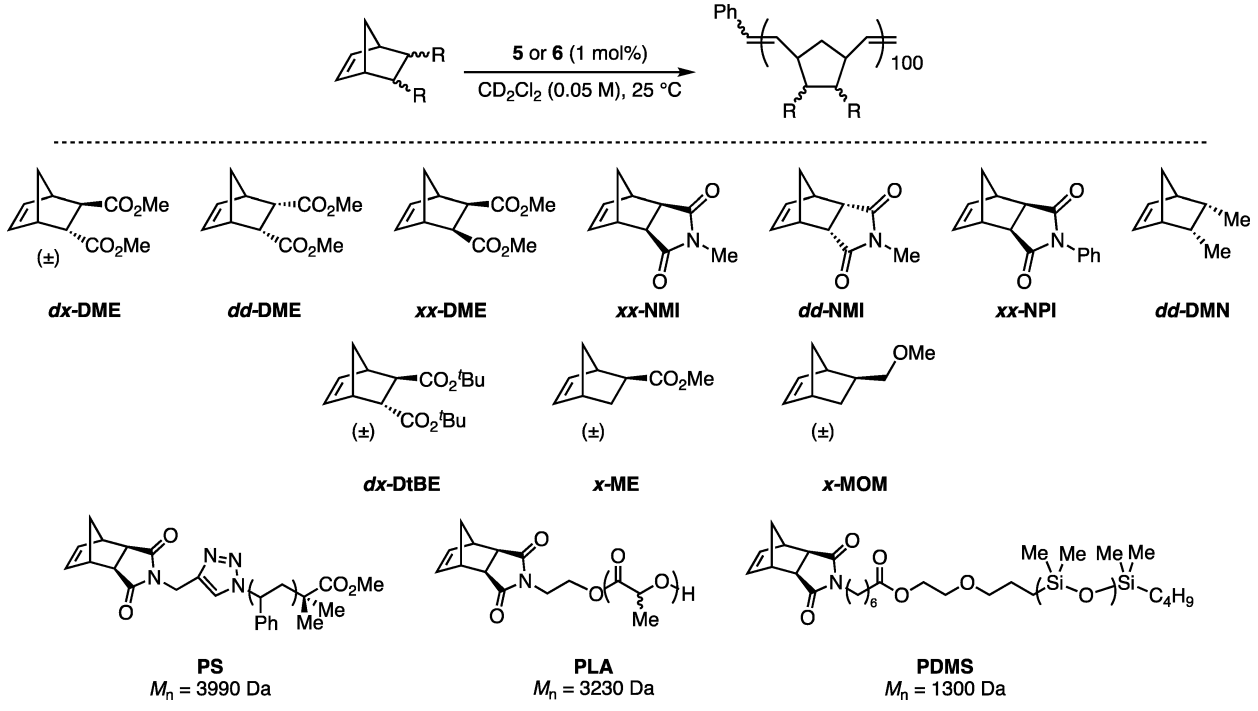

	5 (k_{obs}, $s^{-1} \times 10^3$)	6 (k_{obs}, $s^{-1} \times 10^3$)	Relative rates (k_{obs}(5)/k_{obs}(6))
***dx*-DME**	8.02	1.56	5.1
***dd*-DME**	0.65	0.39	1.7
***xx*-DME**	18.6	5.15	3.6
***xx*-NMI**	28.3	22.1	1.3
***dd*-NMI**	0.3	0.07	4.3
***xx*-NPI**	13.5	9.64	1.4
***x*-ME**	106	29.6	3.6
***x*-MOM**[a]	14.4	4.1	3.5
***dx*-DtBE**	1.3	0.1	13
***dd*-DMN**[a]	12.0	13.0	0.9
PS (3 kDa)	2.1	2.2	1.0
PLA (3.2 kDa)	8.6	8.4	1.0
PDMS (1.3 kDa)	10.8	9.8	1.16

[a]Rate constants measured at 0 °C.

oligomeric chain bound to the Ru center. All three monomers showed temperature-dependent chelation, but the symmetry of ***xx*-DME** presented a simpler system to analyze. The variable temperature NMR array of **5-*xx*-DME** is shown in Figure 7: below −20 °C, two sharp peaks corresponding to the free (8.6 ppm) and Ru-bound (7.9 ppm) pyridine resonances were visible. As the temperature increased, these peaks broadened and eventually coalesced around 15 °C. The complex **6-*xx*-DME** showed a lower coalescence temperature (0 °C for **6**) and a larger equilibrium favoring the chelated state. This phenomenon is attributed to the steric bulk of the SIPr ligand that repels the alkylidene (as part of the growing polymer chain) forcing it into a position to chelate to the Ru center. NMR line shape analysis[25] allowed us to estimate both the frequency of exchange and the equilibrium between both states. Under catalytically relevant concentrations (typically >1 mM), the majority of the Ru species was chelated, leading to a ground state stabilization that results in slower rates of polymerization for chelating monomers. The frequency of exchange was estimated to be in excess of 100 s^{-1} at 25 °C, and so the ligand exchange was much more rapid than propagation (see SI for simulated NMR spectra). In contrast, the oligomer bound Ru species **5-*xx*-NMI** or **6-*xx*-NMI** both show two distinct resonances for the pyridine ligands over a similar temperature range (−20 to +25 °C) indicating that the *exo*-substituted imide does not chelate to the metal center (see SI for VT spectra).

From the pyridine bound state, an associative interchange between the ligand and the chelating ester could proceed through a single, ordered transition state in an associative interchange mechanism. The associative interchange mechanism requires the pyridine ligand to approach the Ru center trans to the alkylidene ligand to open the chelating ring. The different values of K_1 for **5** and **6** show that this position is hindered by the aryl rings of the NHC (Figure 3), and so the exchange between the chelated and pyridine-bound states would be expected to be slower for **6-*xx*-DME** than for **5-*xx*-DME**. However, the calculated frequencies of exchange were faster for **6-*xx*-DME** than for **5-*xx*-DME**, inconsistent with an associative exchange. In contrast, a dissociative exchange would

DOI: 10.1021/jacs.9b08835
J. Am. Chem. Soc. XXXX, XXX, XXX−XXX

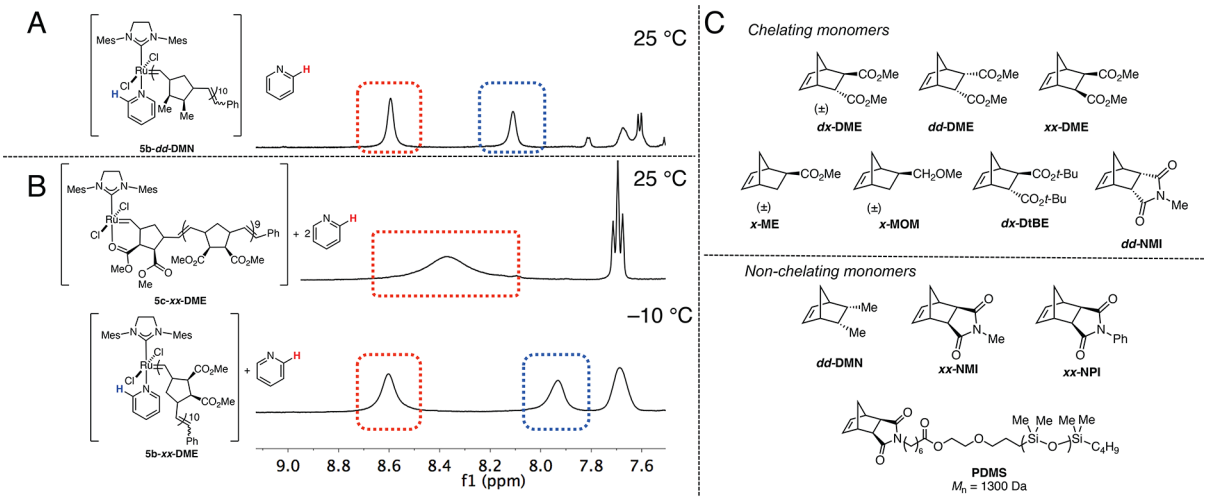

Figure 6. (A) ^{1}H NMR spectrum showing two pyridine resonances for the free (highlighted in red) and bound (highlighted in blue) pyridine resonances for the oligo(**dd-DMN**) bound Ru catalyst. (B) ^{1}H NMR spectra showing the coalescence of the free and bound pyridine resonances for **5c-*xx*-DME** at 25 °C (top), and the resolution of those resonances at −10 °C (bottom). (C) Different monomer types classified by chelating ability.

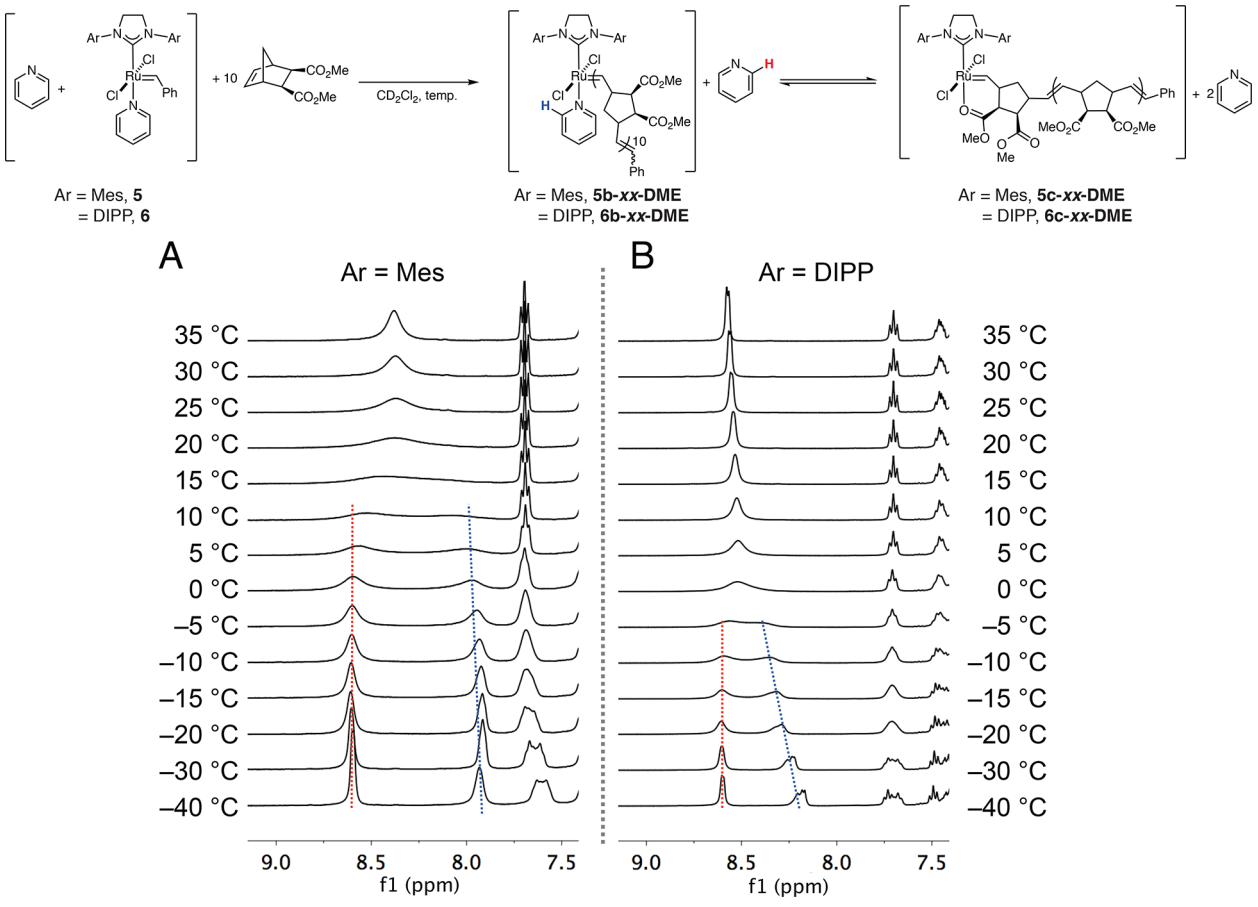

Figure 7. Variable temperature ^{1}H NMR array (400 MHz) showing the coalescence of free (8.6 ppm, highlighted with a red line) and bound (8.2–7.9 ppm, highlighted with a blue line) pyridine signals for **5-*xx*-DME** (A), **6-*xx*-DME** (B).

proceed through the opening of the chelating metallacycle, followed by coordination of the pyridine ligand (Figure 8). This process is expected to be accelerated as the chelating esters come into closer proximity to the Ru center due to steric repulsion by the NHC (Figure 8).

These higher Ru concentrations were also amendable to monitoring the initiation of the Ru catalysts. At 0 °C, the measured values for initiation (k_i) were not hindered by the catalyst sterics for *exo* substituted monomers ***xx*-NMI** and ***xx*-DME** for both **5** and **6** (Table 3, Scheme 3); the initiation of **6** with ***xx*-NMI** was observed to be *faster* than that for **5**. In

DOI: 10.1021/jacs.9b08835
J. Am. Chem. Soc. XXXX, XXX, XXX−XXX

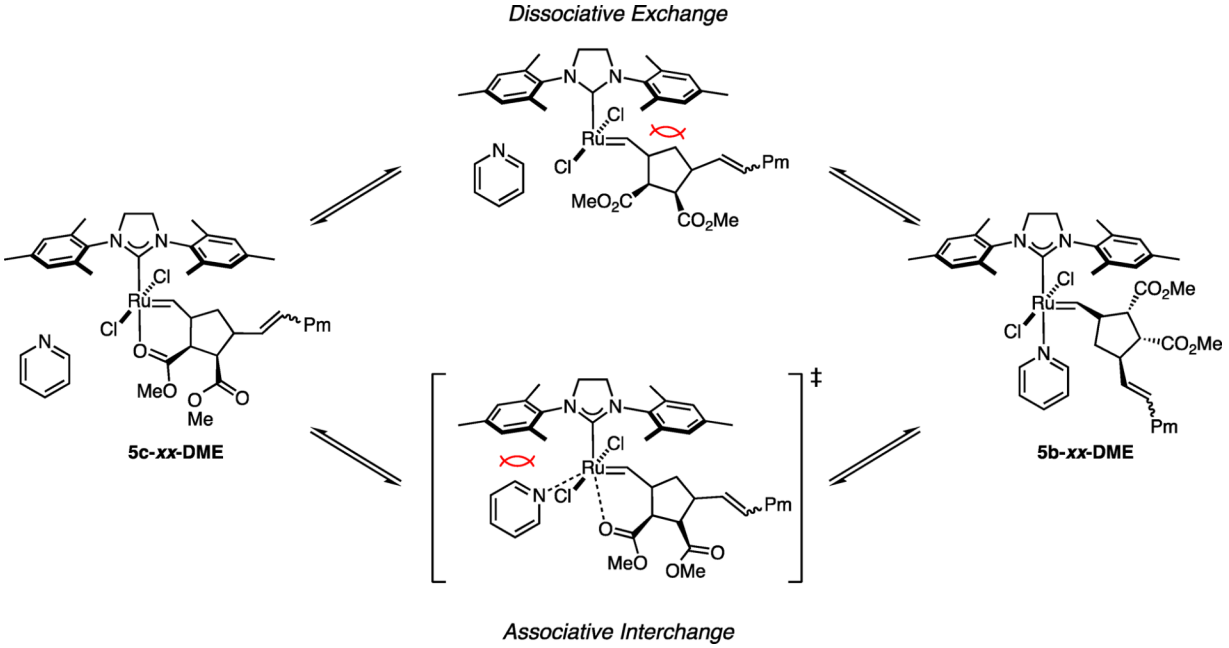

Figure 8. Two mechanistic proposals for the formation of the chelate ring, an associative exchange, and a dissociative exchange (favored).

Table 3. Initiation Rate Constants for Different Geometrical Isomers of Norbornene

Monomer	**5** ($k_{obs} \times 10^3$)	**6** ($k_{obs} \times 10^3$)
***xx*-DME**	k_i = 12(1) s^{-1}	k_i = 13(1) s^{-1}
***xx*-NMI**	k_i = 11(2) s^{-1}	k_i = 16(1) s^{-1}
***dd*-DME**	k_i = 6.0(5) s^{-1}	k_i = 2.0(3) s^{-1}
***dd*-NMI**	k_i = 2.9(2) s^{-1}	k_i = 1.1(2) s^{-1}

contrast, both catalysts initiated more slowly in the presence of the *endo* isomers ***dd*-DME** and ***dd*-NMI**, with **6** initiating less rapidly than **5**. The contrasting rates of initiation indicated that the monomer geometry is also important in determining the rates of polymerization, as the approach of the monomer and the subsequent cycloaddition were affected by the geometry of the norbornene substituents.

Steric clash between the approaching monomer and the Ru catalyst is not expected to be the origin of this phenomenon, since the approach of metal carbenes (and other electrophiles) to the *endo* face of the monomer is known to be disfavored relative to the approach to the exo face. Several titanium metallacylobutanes have been isolated and characterized that exhibit this preference.[26] Instead, the differences in initiation rates can be rationalized by the induction of strain into the norbornene ring system, as shown in Figure 9. The Ru alkylidene approaches the *exo* face of the norbornene monomer, and the olefinic protons are pushed down as the cycloaddition proceeds.

For *endo* substituted monomers, the five-membered ring (highlighted in blue) has four cis substituents (highlighted in bold) which destabilizes the transition state and slows the rate of metathesis. For *exo* monomers, this interaction is avoided and the rates of initiation are faster. The opening of the chelate ring is still an important step that influences the rate of polymerization (compare the rates of ROMP for ***xx*-DME** between **5** and **6**), but the structure of the monomer influences the rate of polymerization beyond providing an appropriate geometry for chelation and suggests that the cycloaddition step is the rate-determining step of ROMP.

We next used a kinetic isotope effect (KIE) as a mechanistic probe. We initially hypothesized that a rate-limiting cycloaddition step would exhibit an inverse secondary KIE, in contrast to a rate-limiting olefin binding step, and so the two steps could thus be differentiated. Several metathesis-active Ru complexes have been characterized in the solid state with olefins bound to the Ru center. The C═C bond lengths of the coordinated olefins did not differ significantly from the average C═C bond length (1.34 Å) for both side- and bottom-bound complexes. In solution, the ^{1}H NMR resonances of the bound olefinic protons shifted upfield significantly, up to several ppm for the sidebound olefins. While these ground state structures do not necessarily reflect the transition state structures, it is

Scheme 3

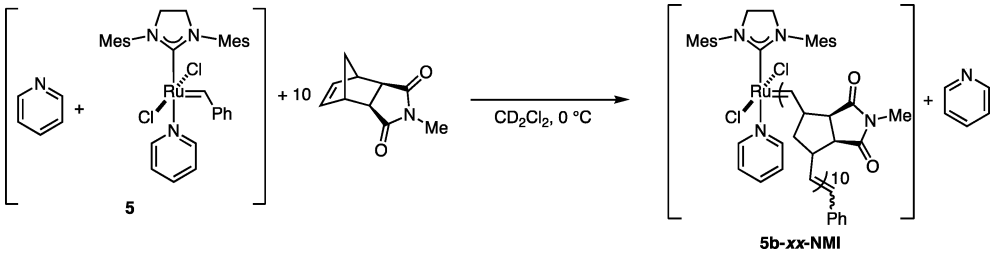

DOI: 10.1021/jacs.9b08835
J. Am. Chem. Soc. XXXX, XXX, XXX−XXX

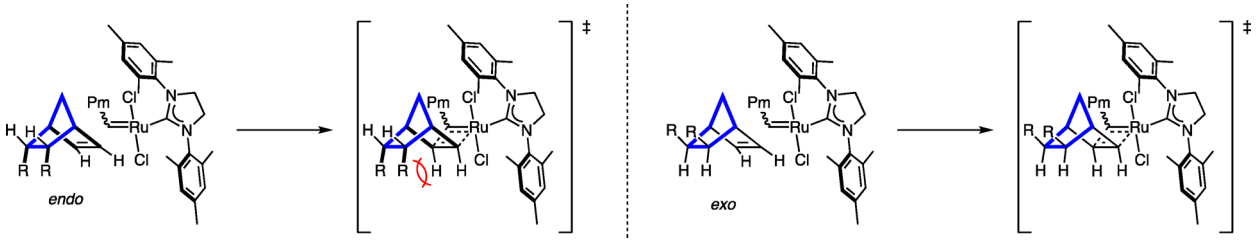

Figure 9. Proposed origin of rate differences for initiation for exo and endo substituted monomers.

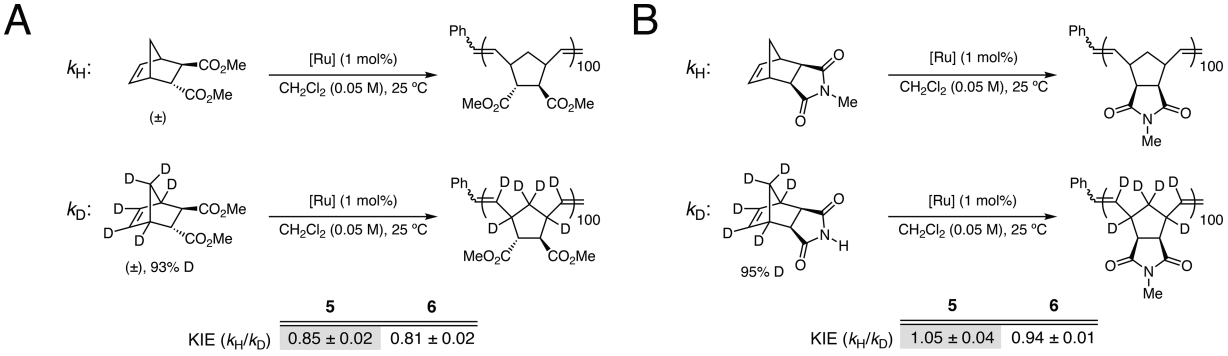

Figure 10. Kinetic isotope effects for both a chelating (A) and a nonchelating (B) monomer. Each measured value represents a weighted average of at least five independent rate measurements for each isotopologue at 25 °C.

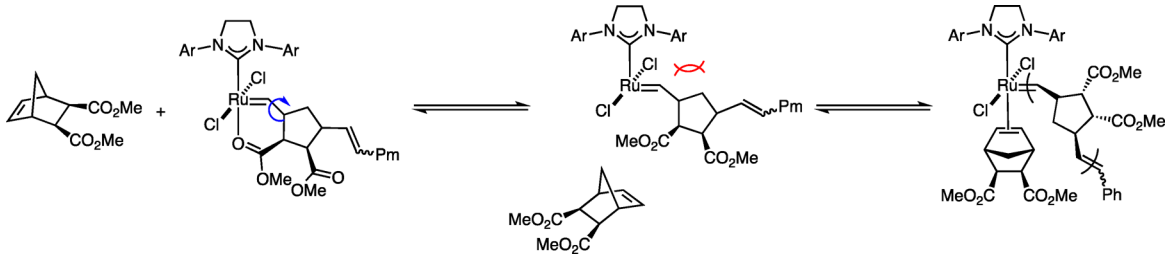

Figure 11. Ring opening of the chelate prior to monomer coordination.

unlikely that a significant elongation of the C═C bond occurs at the transition state between free and bound olefin, and so an inverse secondary KIE is not likely to be a result of olefin binding.[27−29] For third generation catalysts ligated by DMAP, the slow step of the catalytic pathway was proposed to be the olefin association step.[14] In contrast, the dynamics of ligand exchange for the pyridine complexes are very rapid and suggest that the rate-limiting step lies further along the reaction pathway. For the first generation Ru metathesis catalyst, a primary secondary KIE (1.7) has been observed in support of the decomposition of the ruthenacyclobutane intermediate.[30] Using mass spectrometry, Chen and co-workers observed a small secondary KIE of 1.04(4) for the ring opening of norbornene with a deuterated benzylidene in the gas phase.[31] We prepared two different types of isotopically enriched monomers: ***dx*-DME-d_6** for the chelating monomer and ***xx*-NMI-d_6** as a nonchelating monomer. Independent rate measurements were made for each isotopologue with each catalyst at 25 °C (Figure 10).

For ***dx*-DME**, an inverse secondary KIE was observed for both catalysts (Figure 10a) and the magnitude of the KIE increased with the increasing bulk of the NHC. In contrast, the polymerization of ***xx*-NMI** did not exhibit significant KIEs: values around unity were measured for both catalysts (Figure 9b), suggesting that the observed KIEs for ***dx*-DME** were not a result of olefin binding or cycloaddition. Instead, the observed isotope effects for ***dx*-DME** may be classified as steric KIEs, suggesting two possibilities: an associative type mechanism for monomer coordinating to the Ru center or a dissociative mechanism involving a crowded Ru center (Figure 10). For the dissociative pathway, the alkylidene must rotate up into the aryl ring of the NHC ligand, which is hindered by the increasing size of the aryl rings on the NHC ligand, leading to the increasing magnitude of the KIE. The steric profile of the NHC has a smaller effect on the propagating Ru species for nonchelating monomers, and the smaller KIEs for ***xx*-NMI** are consistent with this mechanism. The steric bulk of **6** had a small effect on the rate of polymerization of ***xx*-NMI**, as a small KIE was observed (0.94(1)) which could be attributed to monomer coordination to the Ru species. In contrast, an associative interchange mechanism could also rationalize the observed KIE for ***dx*-DME**, where steric clash between the NHC and the incoming monomer would be alleviated by the shorter C−D bonds. Ru benzylidene precatalysts like **3** have been proposed to initiate via an associative interchange mechanism.[32] In particular, Plenio and co-workers showed that initiation of **3** and related derivatives is a combination of both an associative interchange and dissociative exchange mechanism, with smaller substrates favoring the associative interchange pathway.[33] Lloyd-Jones and co-workers have also

DOI: 10.1021/jacs.9b08835
J. Am. Chem. Soc. XXXX, XXX, XXX−XXX

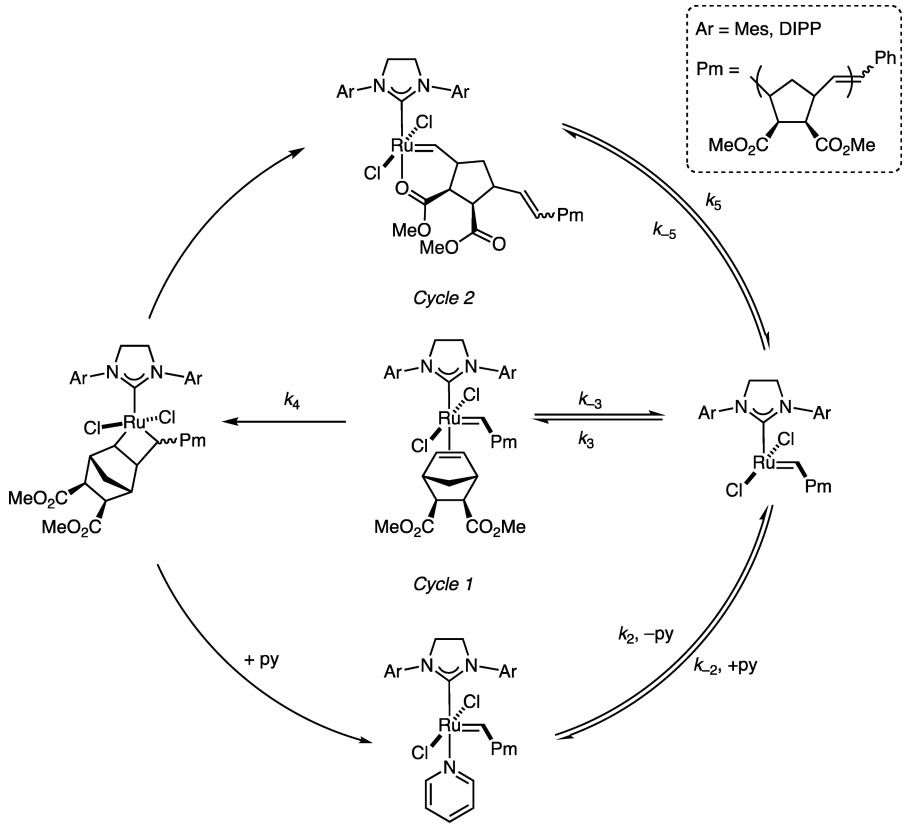

Figure 12. Proposed mechanism for the ROMP of norbornene monomers.

shown that the reaction of third generation Ru catalysts with vinyl ethers proceeds via a combination of both mechanisms, with an associative interchange mechanism dominating at higher substrate concentration,[34] supporting calculations by Grela. For larger substrates such as norbornene and other disubstituted olefins, both experimental[33] and computational[13,16] evidence support a dissociative mechanism. For ROMP, the steric size of the NHC has a small effect on the rate of polymerization for nonchelating monomers (Table 2) which is consistent with a dissociative mechanism. For chelating monomers, there is a pronounced steric effect on the rates of polymerization and on the position of the chelating equilibrium, and so the isotope effect may be assigned to the interaction between the polymer chain and the NHC. For bottom-bound metallacycles, the alkylidene must rotate up into the aryl rings of the NHC, congestion which would be alleviated by the shorter C–D bonds of the deuterated polymer chain (Figure 11).

The polymerizations of both monomer types show a first-order dependence on monomer concentration, and an inverse first-order dependence on pyridine concentration. Interestingly, the order in catalyst has been shown to be zero, as established by Guirronnet and co-workers, and was assigned to the cancellation of $[Ru]_0$ and [py] terms in the rate law. The dissociative mechanism (cycle 1, Figure 12) fits with a competitive inhibition model with the rate law shown in eq 1. For nonchelating monomers, fast and reversible pyridine dissociation produces a reactive 14-electron complex which can then bind substrate and proceed with a productive metathesis event, similar to the established mechanism for other Ru catalysts. Since we have estimated K_2 to be on the order of 10^{-6}, the rate law shown in eq 1 can be reduced to the simpler form in eq 2 when $K_m[py] \gg K_2K_m$ and $K_2[M]_0$. This rate law is consistent with the experimental observations that the polymerizations are first-order in monomer, are inverse first-order in pyridine, and can rationalize the observed zero-order dependence on $[Ru]_0$. Additionally, we have observed a dependence on $[Ru]_0$ at lower concentrations of **5** (and subsequently lower concentrations of pyridine) such that $K_m[py] \approx K_2K_m$ and $K_2[M]_0$. The steric size of the NHC ligand has little effect on the observed rates of polymerization for nonchelating monomers in support of a dissociative mechanism for propagation. While *exo*-substituted imides are geometrically unable to chelate to the metal center, the steric size of the substituent interferes with the approach of the monomer to the metal center, slowing the rate of polymerization (***xx*-NMI** vs ***xx*-NPI**, Table 2).

$$\frac{-\mathrm{d}[M]}{\mathrm{d}t} = \frac{k_4[Ru]_0[M]_0}{K_m\left(1 + \frac{[py]}{K_2}\right) + [M]_0} = \frac{k_4K_2[Ru]_0[M]_0}{k_2K_m + K_m[py] + K_2[M]_0} \quad (1)$$

$$K_m = \frac{k_{-3} + k_4}{k_3}$$

$$\frac{-\mathrm{d}[M]}{\mathrm{d}t} \approx \frac{k_4K_2[Ru]_0[M]_0}{K_m[py]} \quad (2)$$

The mechanism of polymerization of chelating monomers has an additional equilibrium for the opening of the chelated metallacycle (cycle 2, Figure 12). Rapid ligand exchange between the pyridine-bound Ru species and the chelated

DOI: 10.1021/jacs.9b08835
J. Am. Chem. Soc. XXXX, XXX, XXX–XXX

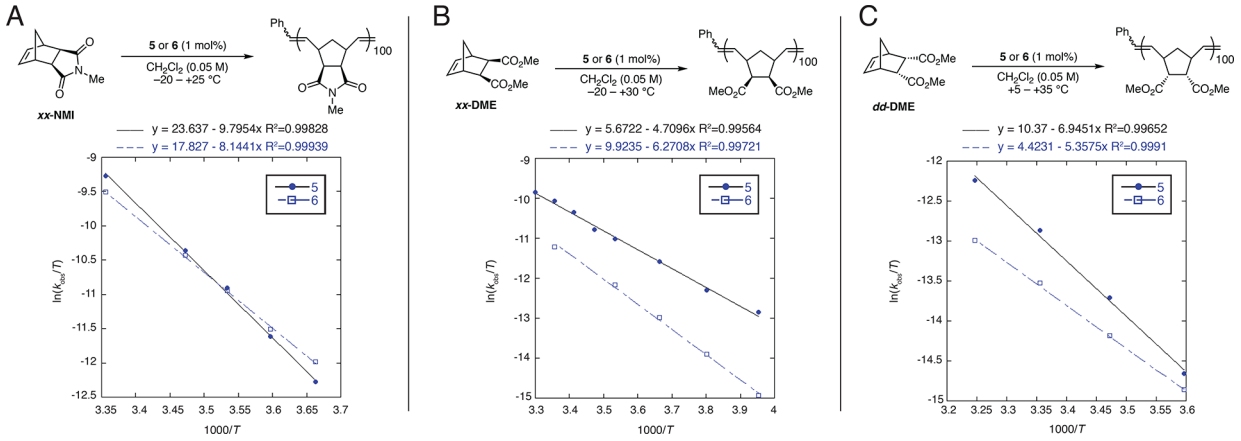

Figure 13. Eyring plots for the polymerization of ***xx*-NMI** with **5** and **6** (A), ***xx*-DME** with **5** and **6** (B), and ***dd*-DME** with **5** and **6** (C).

Table 4. Activation Parameters for the Polymerization of Chelating and Non-Chelating Monomers Using 5 and 6

	xx-NMI	*xx*-DME	*dd*-DME
5	$\Delta S^{\ddagger} = -8 \pm 2$ J/mol·K	$\Delta S^{\ddagger} = -150 \pm 6$ J/mol·K	$\Delta S^{\ddagger} = -111 \pm 8$ J/mol·K
	$\Delta H^{\ddagger} = 19 \pm 0.4$ kcal/mol	$\Delta H^{\ddagger} = 9.3 \pm 0.3$ kcal/mol	$\Delta H^{\ddagger} = 13.8 \pm 0.6$ kcal/mol
6	$\Delta S^{\ddagger} = -49 \pm 3$ J/mol·K	$\Delta S^{\ddagger} = -115 \pm 6$ J/mol·K	$\Delta S^{\ddagger} = -160 \pm 3$ J/mol·K
	$\Delta H^{\ddagger} = 16 \pm 2$ kcal/mol	$\Delta H^{\ddagger} = 12.3 \pm 0.4$ kcal/mol	$\Delta H^{\ddagger} = 10.6 \pm 0.3$ kcal/mol

species proceeds through the 14-electron intermediate, which can proceed through a productive metathesis event, adding to the growing polymer chain. For chelating monomers, the steric size of the NHC ligand has a pronounced influence on the rates of polymerization, since K_5 favors the chelated resting state due to steric repulsion between the alkylidene and the NHC (eq 3). This effect is maximized when both the chelating group and the NHC are large, as demonstrated by the large differences in the rate of polymerization of ***dx*-D^{t}BE** for **5** and **6** (Table 2).

$$\frac{-\mathrm{d[M]}}{\mathrm{d}t} = \frac{k_4 K_2 K_5 [\mathrm{Ru}]_0 [\mathrm{M}]}{K_m K_5 [\mathrm{py}] + K_2 K_m + K_2 K_5 K_m + K_2 K_5 [\mathrm{M}]} \quad (3)$$

Eyring analysis provided another means of distinguishing the two monomer types. It is difficult to deconvolute the activation parameters of a multistep mechanism,[35] and so the measured parameters reflect contributions from several reversible steps. The ring opening of chelated Ru catalysts has been extensively studied using Eyring analysis, and the measured activation parameters differ from those observed for phosphine ligated second generation Ru catalysts[36] particularly with respect to activation entropies. Large, negative values of $\Delta S^{\ddagger}$ have been observed for the initiation of **3** and its related derivatives using butyl vinyl ether[33] in contrast to the positive values of $\Delta S^{\ddagger}$ for phosphine catalysts that are indicative of phosphine dissociation. These entropies have been used to support an associative exchange mechanism, but they are also consistent with a dissociative mechanism proceeding through a rate-limiting olefin association step.[37]

The temperature profile for the polymerization of ***xx*-NMI** using **5** is shown in Figure 13, with activation parameters compiled in Table 4. A small, negative entropy of activation ($\Delta S^{\ddagger}$) was determined (−8(2) J/mol·K) with an enthalpy of activation ($\Delta H^{\ddagger}$) of 19.0(4) kcal/mol. The temperature profile for the polymerization of ***xx*-NMI** with **6** is similar over the same temperature range, further highlighting the similarities between the two catalysts. A larger, negative value of $\Delta S^{\ddagger}$ (−49(3) J/mol·K) was determined for the ROMP of ***xx*-NMI** with **6**, with a $\Delta H^{\ddagger}$ of 16(2) kcal/mol. The ROMP of ***xx*-DME** was evaluated over a similar temperature range, and a much larger magnitude of $\Delta S^{\ddagger}$ was determined (−150 ± 5) J/mol·K) with a $\Delta H^{\ddagger}$ of 9.3(3) kcal/mol.

Entropy is a much larger contributor to the activation energy required for chelating monomers, and similarly large values have been measured for the initiation of **3**. The opening of the chelate ring has a minor entropic cost compared to monomer association, and so the composite value of $\Delta S^{\ddagger}$ most strongly reflects the associative step. For the pyridine bound resting state, the reversible dissociation of the pyridine ligand makes a much larger contribution to the entropy, and so the composite values of $\Delta S^{\ddagger}$ are less negative (near zero). Both *exo* and *endo* substituted monomers (***xx*-DME** and ***dd*-DME**, Table 4) exhibited similarly large, negative activation entropies for polymerization, supporting similar mechanisms that proceed from a chelated Ru species.

The mechanistic features described above are relevant to both our own and others[38] recent work on variably grafted polymers. A variety of different polymer architectures can be accessed rapidly and reliably by selecting an appropriate macromonomer and small molecule diluent pair. The most important step in these polymerizations is the crossover step, which controls the rate at which both monomers are incorporated into the growing polymer side chain. Monomer/macromonomer pairs are chosen based on their homopolymerization rates, and the reactivity ratios are then evaluated to ensure that the desired polymer sequence (blocky, gradient, or random) can be synthesized. This approach is highly tunable, given the synthetic accessibility of a wide variety of small molecule diluents and macromonomers. The reactivity ratios are affected by the structure of the propagating Ru center, which is in turn affected by the nature of the monomer, according to the Mayo−Lewis model. A copolymerization of ***xx*-NMI** and ***dd*-NMI** not only demonstrated the differences between the propagation of both monomers but

DOI: 10.1021/jacs.9b08835
J. Am. Chem. Soc. XXXX, XXX, XXX−XXX

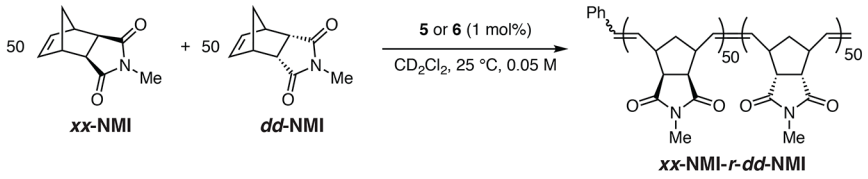

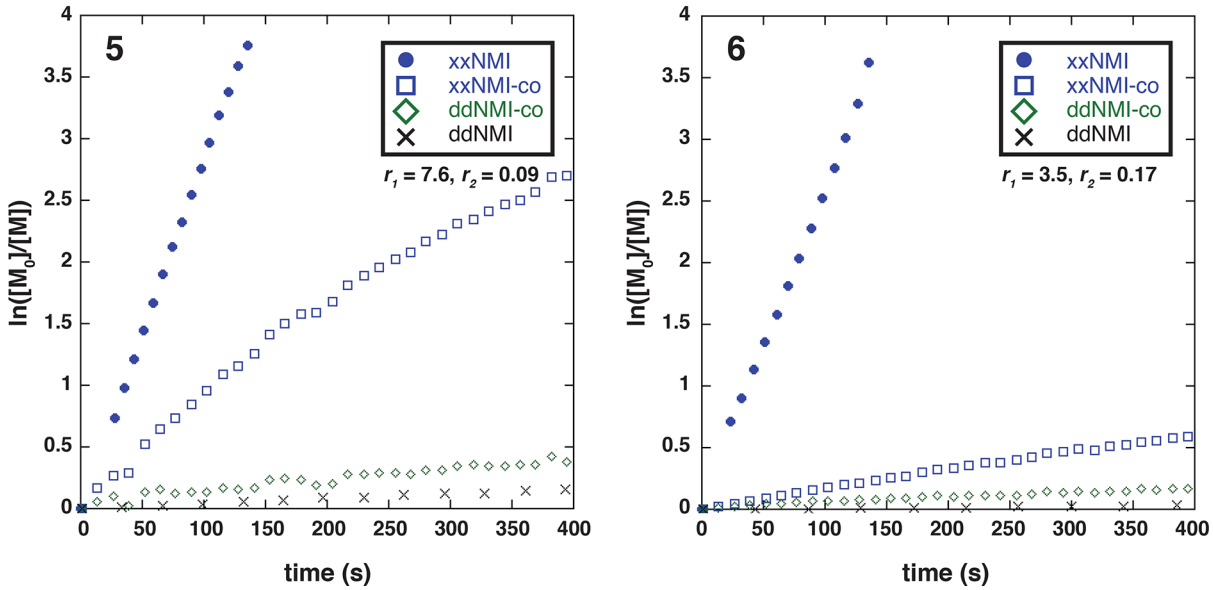

Figure 14. Plots of ln([M_0]/[M]) against time for the copolymerization of ***xx*-NMI** (blue, □) and ***dd*-NMI** (green, ◇) using **5** (left) or **6** (right), compared to the homopolymerization rates of each monomer (***xx*-NMI** (blue, ●) and ***dd*-NMI** (×)).

also showed how the structure of the propagating catalyst affects the rate of polymerization. When the Ru site is chelated, the addition of the next monomer into the polymer chain is hindered: the incorporation of ***xx*-NMI** into the polymer chain is slowed by the presence of ***dd*-NMI** relative to its homopolymerization rate. Conversely, the presence of the nonchelated Ru species accelerates the incorporation of the subsequent monomer: the consumption of ***dd*-NMI** is accelerated relative to its homopolymerization rate (Figure 14). This effect is exaggerated when **6** is used as the initiator, since the chelation is enforced more strongly.

The crossover rate constants (k_{12} and k_{21}) and subsequent reactivity ratios (r_1 and r_2) are strongly affected by the structure of the catalyst, through enforcing the growing polymer chain to chelate to the Ru center. Linear regression allowed us to determine the reactivity ratios for the copolymerization of ***xx*-NMI** and ***dd*-NMI**, highlighting the difference between **5** and **6** and demonstrating how the chelating ability of the polymer chain affects the reactivity of the Ru center. The values of r_1 and r_2 are much more disparate for **5** than for **6**, which can be attributed to the strongly chelated Ru center present when **6** is used as the initiator.

CONCLUSIONS

The mechanism of Ru-catalyzed metathesis polymerization has been examined as a function of catalyst structure, providing experimental evidence for a number of mechanistic features. Importantly, cyclic olefin monomers were classified as either "chelating" or "nonchelating" in reference to their ability to form a stabilized metallacycle as the resting state of the active Ru center. The influence of the steric environment of the catalyst on chelation was demonstrated with different monomer types, as chelation can be enforced by repulsion between the growing polymer chain and the substituents of the NHC ligand. In addition, the structure of the monomer was also shown to be an important factor that influences the rate of polymerization. Several key features distinguished the chelating and nonchelating monomers from one another including homopolymerization rates, initiation rates, activation parameters, and KIEs, highlighting the influence that the monomer structure imparts on the structure and reactivity of the propagating Ru center. These results provide additional mechanistic insights into the third generation mediated ROMP and are particularly interesting in the context of our continuing work on the design and synthesis of new polymers and materials.

ASSOCIATED CONTENT

Supporting Information

The Supporting Information is available free of charge on the ACS Publications website at DOI: 10.1021/jacs.9b08835.

Experimental Procedures, NMR spectra, additional kinetic plots (PDF)

Crystallographic information file for **6a** (CIF)

AUTHOR INFORMATION

Corresponding Author

*rhg@caltech.edu

ORCID

Tzu-Pin Lin: 0000-0001-7041-7213

Robert H. Grubbs: 0000-0002-0057-7817

Notes

The authors declare no competing financial interest.

DOI: 10.1021/jacs.9b08835
J. Am. Chem. Soc. XXXX, XXX, XXX−XXX

■ ACKNOWLEDGMENTS

W.J.W. gratefully acknowledges the Arnold O. Beckman postdoctoral fellowship for financial support. We thank Dr. David VanderVelde for assistance with NMR experiments, Dr. Michael Takase for assistance with X-ray crystallography, and Dr. Mona Shagholi for assistance with HRMS. We are also indebted to Drs. Tonia Ahmed, Adam Johns, Allegra Liberman-Martin, Chris Marotta, and Mr. Jiaming Li for helpful discussions and assistance with preparing this manuscript. We thank Materia Inc. for the generous donation of Ru metathesis catalysts. We gratefully acknowledge Dr. Jase Gehring for assistance with preparing figures.

■ REFERENCES

(1) Handbook of Metathesis, Vol. *1*: *Catalyst Development and Mechanism*, 2nd ed. https://www.wiley.com/en-us/Handbook+of+Metathesis%2C+Vol.+1%3A+Catalyst+Development+and+Mechanism%2C+2nd+Edition-p-9783527339488 (accessed Feb 22, 2018).

(2) Scholl, M.; Ding, S.; Lee, C. W.; Grubbs, R. H. Synthesis and Activity of a New Generation of Ruthenium-Based Olefin Metathesis Catalysts Coordinated with 1,3-Dimesityl-4,5-Dihydroimidazol-2-Ylidene Ligands. *Org. Lett.* **1999**, *1* (6), 953−956.

(3) Garber, S. B.; Kingsbury, J. S.; Gray, B. L.; Hoveyda, A. H. Efficient and Recyclable Monomeric and Dendritic Ru-Based Metathesis Catalysts. *J. Am. Chem. Soc.* **2000**, *122* (34), 8168−8179.

(4) Gessler, S.; Randl, S.; Blechert, S. Synthesis and Metathesis Reactions of a Phosphine-Free Dihydroimidazole Carbene Ruthenium Complex. *Tetrahedron Lett.* **2000**, *41* (51), 9973−9976.

(5) Endo, K.; Grubbs, R. H. Chelated Ruthenium Catalysts for Z-Selective Olefin Metathesis. *J. Am. Chem. Soc.* **2011**, *133* (22), 8525−8527.

(6) Keitz, B. K.; Endo, K.; Patel, P. R.; Herbert, M. B.; Grubbs, R. H. Improved Ruthenium Catalysts for Z-Selective Olefin Metathesis. *J. Am. Chem. Soc.* **2012**, *134* (1), 693−699.

(7) Sanford, M. S.; Love, J. A.; Grubbs, R. H. A Versatile Precursor for the Synthesis of New Ruthenium Olefin Metathesis Catalysts. *Organometallics* **2001**, *20* (25), 5314−5318.

(8) Choi, T.-L.; Grubbs, R. H. Controlled Living Ring-Opening-Metathesis Polymerization by a Fast-Initiating Ruthenium Catalyst. *Angew. Chem., Int. Ed.* **2003**, *42* (15), 1743−1746.

(9) Handbook of Metathesis, Vol. *3*: *Polymer Synthesis*, 2 nd ed. https://www.wiley.com/en-us/Handbook+of+Metathesis%2C+Vol.+3%3A+Polymer+Synthesis%2C+2nd+Edition-p-9783527339501 (accessed May 9, 2019).

(10) Sanford, M. S.; Love, J. A.; Grubbs, R. H. Mechanism and Activity of Ruthenium Olefin Metathesis Catalysts. *J. Am. Chem. Soc.* **2001**, *123* (27), 6543−6554.

(11) Slugovc, C.; Demel, S.; Riegler, S.; Hobisch, J.; Stelzer, F. The Resting State Makes the Difference: The Influence of the Anchor Group in the ROMP of Norbornene Derivatives. *Macromol. Rapid Commun.* **2004**, *25* (3), 475−480.

(12) Walsh, D. J.; Lau, S. H.; Hyatt, M. G.; Guironnet, D. Kinetic Study of Living Ring-Opening Metathesis Polymerization with Third-Generation Grubbs Catalysts. *J. Am. Chem. Soc.* **2017**, *139* (39), 13644−13647.

(13) Trzaskowski, B.; Grela, K. Structural and Mechanistic Basis of the Fast Metathesis Initiation by a Six-Coordinated Ruthenium Catalyst. *Organometallics* **2013**, *32* (13), 3625−3630.

(14) Dunbar, M.; Balof, S.; LaBeaud, L.; Yu, B.; Lowe, A.; Valente, E.; Schanz, H.-J. Improved Molecular Weight Control in Ring-Opening Metathesis Polymerization (ROMP) Reactions with Ru-Based Olefin Metathesis Catalysts Using N Donors and Acid: A Kinetic and Mechanistic Investigation. *Chem. - Eur. J.* **2009**, *15* (45), 12435−12446.

(15) Radzinski, S. C.; Foster, J. C.; Chapleski, R. C.; Troya, D.; Matson, J. B. Bottlebrush Polymer Synthesis by Ring-Opening Metathesis Polymerization: The Significance of the Anchor Group. *J. Am. Chem. Soc.* **2016**, *138* (22), 6998−7004.

(16) Chang, A. B.; Lin, T.-P.; Thompson, N. B.; Luo, S.-X.; Liberman-Martin, A. L.; Chen, H.-Y.; Lee, B.; Grubbs, R. H. Design, Synthesis, and Self-Assembly of Polymers with Tailored Graft Distributions. *J. Am. Chem. Soc.* **2017**, *139* (48), 17683−17693.

(17) Leitao, E. M.; Piers, W. E.; Parvez, M. A Thermally Robust Ruthenium Phosphonium Alkylidene Catalyst — the Effect of More Bulky N-Heterocyclic Carbene Ligands on Catalyst Performance in Olefin Metathesis Reactions. *Can. J. Chem.* **2013**, *91* (10), 935−942.

(18) Perrin, C. L.; Dwyer, T. J. Application of Two-Dimensional NMR to Kinetics of Chemical Exchange. *Chem. Rev.* **1990**, *90* (6), 935−967.

(19) Kitamoto, Y.; Kobayashi, F.; Suzuki, T.; Miyata, Y.; Kita, H.; Funaki, K.; Oi, S. Investigation of the Lewis Acidic Behaviour of an Oxygen-Bridged Planarized Triphenylborane toward Amines and the Properties of Their Lewis Acid-Base Adducts. *Dalton Trans* **2019**, *48* (6), 2118−2127.

(20) Hong, S. H.; Wenzel, A. G.; Salguero, T. T.; Day, M. W.; Grubbs, R. H. Decomposition of Ruthenium Olefin Metathesis Catalysts. *J. Am. Chem. Soc.* **2007**, *129* (25), 7961−7968.

(21) Bailey, G. A.; Foscato, M.; Higman, C. S.; Day, C. S.; Jensen, V. R.; Fogg, D. E. Bimolecular Coupling as a Vector for Decomposition of Fast-Initiating Olefin Metathesis Catalysts. *J. Am. Chem. Soc.* **2018**, *140* (22), 6931−6944.

(22) Macnaughtan, M. L.; Gary, J. B.; Gerlach, D. L.; Johnson, M. J. A.; Kampf, J. W. Cross-Metathesis of Vinyl Halides. Scope and Limitations of Ruthenium-Based Catalysts. *Organometallics* **2009**, *28* (9), 2880−2887.

(23) Benoit, R. L.; Fréchette, M.; Lefebvre, D. 2,6-Di- *Tert* -Butylpyridine: An Unusually Weak Base in Dimethylsulfoxide. *Can. J. Chem.* **1988**, *66* (5), 1159−1162.

(24) Brown, H. C.; Kanner, B. 2,6-Di-Butylpyridine—An Unusual Pyridine Base. *J. Am. Chem. Soc.* **1953**, *75* (15), 3865−3865.

(25) Bányai, I. Dynamic NMR for Coordination Chemistry. *New J. Chem.* **2018**, *42* (10), 7569−7581.

(26) Gilliom, L. R.; Grubbs, R. H. Titanacyclobutanes Derived from Strained, Cyclic Olefins: The Living Polymerization of Norbornene. *J. Am. Chem. Soc.* **1986**, *108* (4), 733−742.

(27) Tallarico, J. A.; Bonitatebus, P. J.; Snapper, M. L. Ring-Opening Metathesis. A Ruthenium Catalyst Caught in the Act. *J. Am. Chem. Soc.* **1997**, *119* (30), 7157−7158.

(28) Anderson, D. R.; Hickstein, D. D.; O'Leary, D. J.; Grubbs, R. H. Model Compounds of Ruthenium-Alkene Intermediates in Olefin Metathesis Reactions. *J. Am. Chem. Soc.* **2006**, *128* (26), 8386−8387.

(29) Stewart, I. C.; Benitez, D.; O'Leary, D. J.; Tkatchouk, E.; Day, M. W.; Goddard, W. A.; Grubbs, R. H. Conformations of N-Heterocyclic Carbene Ligands in Ruthenium Complexes Relevant to Olefin Metathesis. *J. Am. Chem. Soc.* **2009**, *131* (5), 1931−1938.

(30) Ulman, M.; Grubbs, R. H. Relative Reaction Rates of Olefin Substrates with Ruthenium(II) Carbene Metathesis Initiators1. *Organometallics* **1998**, *17* (12), 2484−2489.

(31) Adlhart, C.; Hinderling, C.; Baumann, H.; Chen, P. Mechanistic Studies of Olefin Metathesis by Ruthenium Carbene Complexes Using Electrospray Ionization Tandem Mass Spectrometry. *J. Am. Chem. Soc.* **2000**, *122* (34), 8204−8214.

(32) Nelson, D. J.; Percy, J. M. The Influence of Structure on Reactivity in Alkene Metathesis. *Advances in Physical Organic Chemistry*; Elsevier, 2014; Vol. *48*, pp 81−188.

(33) Thiel, V.; Hendann, M.; Wannowius, K.-J.; Plenio, H. On the Mechanism of the Initiation Reaction in Grubbs-Hoveyda Complexes. *J. Am. Chem. Soc.* **2012**, *134* (2), 1104−1114.

(34) Forcina, V.; Garcia-Dominguez, A.; Lloyd-Jones, G. C. Kinetics of Initiation of the Third Generation Grubbs Metathesis Catalyst: Convergent Associative and Dissociative Pathways. *Faraday Discuss.* **2019**, DOI: 10.1039/C9FD00043G.

(35) Espenson, J. H. *Chemical Kinetics and Reaction Mechanisms*, 2nd ed.; McGraw-Hill, 2002.

DOI: 10.1021/jacs.9b08835
J. Am. Chem. Soc. XXXX, XXX, XXX−XXX

(36) Vougioukalakis, G. C.; Grubbs, R. H. Ruthenium-Based Olefin Metathesis Catalysts Coordinated with Unsymmetrical N-Heterocyclic Carbene Ligands: Synthesis, Structure, and Catalytic Activity. *Chem. - Eur. J.* **2008**, *14* (25), 7545−7556.
(37) Hejl, A. *Controlling Olefin Metathesis through Catalyst and Monomer Design*, PhD, California Institute of Technology, 2007.
(38) Jiang, L.; Nykypanchuk, D.; Ribbe, A. E.; Rzayev, J. One-Shot Synthesis and Melt Self-Assembly of Bottlebrush Copolymers with a Gradient Compositional Profile. *ACS Macro Lett.* **2018**, *7* (6), 619−623.

DOI: 10.1021/jacs.9b08835
J. Am. Chem. Soc. XXXX, XXX, XXX−XXX